Fogwater Collector Design and Characterization

Daniel J. Jacob, Rueen-Fang T. Wang, and Richard C. Flagan*

Environmental Engineering Science, Keck Engineering Laboratories, California Institute of Technology, Pasadena, California 91125

■ The detailed characterization of a rotating arm collector to sample ambient fog droplets for chemical analysis is presented. Because of the large volume of sample required, and because fog droplets are of supermicron size and are sensitive to local thermodynamic disturbances, conventional methods for atmospheric aerosol sampling are not suitable for fogwater sampling. Design criteria for fogwater samplers are outlined. Devices used in previous investigations are evaluated in light of these criteria. The design of a rotating arm collector is discussed, and it is shown that this instrument performs adequately in preserving the physical and chemical integrity of the sample at all stages of collection. Limitations in the design due to mechanical constraints are discussed. Results of an in situ calibration experiment using a chemically tagged monodisperse aerosol indicate a size cut of 20-μm diameter.

Introduction

Supermicron particles contribute significantly to the total mass of a dry aerosol (*1*). This contribution increases considerably when the aerosol is wetted, especially under supersaturated conditions in which activated condensation nuclei grow rapidly to form cloud or fog droplets. Whereas the mass loading of an urban aerosol under nonsaturated conditions is of the order of 10^{-4} g m^{-3}, the liquid water content in a cloud or fog ranges from 0.01 to 1 g m^{-3}, with supermicron droplets constituting the bulk of the aerosol mass. In urban environments fogwater has been found to contain extremely high pollutant concentrations, often associated with high acidities (*2*, *3*).

Supermicron particles are difficult to collect efficiently because their inertia may prevent them from following the air streamlines converging toward the inlet of the sampler (*4*). Furthermore, water droplets in the atmosphere are in a fragile thermodynamic balance with the ambient humidity which is very sensitive to perturbations by a sampling device. Conventional methods for collecting samples of total particulate matter may, therefore, lead to sampling biases due to anisokinetic sampling conditions or changes in temperature or pressure. Fog sampling is further complicated by the relatively large sample volume required for the study of the detailed aquatic chemistry. At least 10 mL of sample is needed for the standard inorganic analysis routinely carried out in our fog program (*3*). If the variation in chemical composition throughout the fog event is to be studied, sampling intervals should be short. For a typical liquid water content of 0.1 g m^{-3}, a sampling rate of over 1.7 m^3 min^{-1} is required to collect 10 mL for analysis in an hour. Larger sampling rates are required for the study of light fogs.

A rotating arm collector based on the principle of inertial impaction has been developed and used in our intensive fog sampling program. Major advances in the understanding of fog chemistry and the role of fogs in acid deposition have been made by using this device (*3*, *5*). In a recent field intercomparison study of fogwater collectors (*6*), samples were collected simultaneously with instruments from five different research groups and analyzed for major ions. Ionic concentrations in samples collected by the rotating arm collector and a jet impactor (*7*) agreed within 5%; other collectors gave systematically either higher or lower concentrations. The rotating arm collector was found to collect water efficiently in both light and heavy fogs.

To date, the sampling characteristics of the rotating arm collector have only been qualitatively explored by measuring the change in the droplet size distribution in a cloud chamber which results from its operation. These measurements indicated that the minimum size of particles collected was at least 8 μm but did not provide sufficient resolution to determine the size-dependent collection efficiency (*8*). In this paper we first elaborate on the design criteria relevant to fogwater collection and then present a detailed examination of the design and operation of our rotating arm collector. Constraints on the design due to power requirements and possible sample biases due to aerodynamic heating are explored. Measurements of the collection efficiency as a function of particle size are presented.

Design Criteria for Fogwater Collectors

Size Cut. Fog droplets form by activation of atmospheric particles (condensation nuclei) under supersaturated conditions. At the levels of supersaturation found in the atmosphere, the lower size limit for particles to be activated is of the order of 0.1 μm (*9*). Figure 1 shows how fog formation can shift the size distribution of an urban aerosol; particles in the first mode (below 0.1 μm) are rather unaffected by the condensation process, but most particles in the two higher modes grow by condensation to much larger sizes. Therefore, two types of particles coexist in a fog: (1) supermicron fog droplets and (2) nonactivated, primarily submicron, particles. Being dilute aqueous solutions, fog droplets do not interact with their environment in the same way as the solid or concentrated submicron particles (*10*, *11*). It is, therefore, important that a fogwater sampler differentiate between the two types of particles.

Fog droplets range in size from 1 to 100 μm, with a mass median diameter usually in the range 10–40 μm (*12–15*). The dependence of the fog droplet chemical composition on droplet size has not been rigorously investigated to date; general predictions from droplet growth theory (*16*) are difficult to make because humidities in fogs fluctuate rapidly in a manner that is still poorly understood (*17*, *18*). Large droplets are not necessarily more dilute than smaller droplets because they generally result from condensation on larger nuclei. If the total pollutant burden associated with fogs is to be determined, droplets of all sizes should be collected with the same efficiency. Nonactivated submicron particles represent a very small fraction of the total aerosol mass but they could, if collected, contribute a sizable amount of solutes to the sample and result in a serious bias. A sharp lower size cut in the range 1–10-μm diameter is, therefore, desired. Furthermore, since most of the fog mass is associated with large droplets, droplets up to about 100-μm diameter must be collected without bias.

Three methods are available to collect the large particles while excluding the smaller particles: sedimentation, inertial separation, and removal of smaller particles by

0013-936X/84/0918-0827$01.50/0

Table I. Fogwater Collectors Reported in the Literature

reference	type	impaction velocity, cm s^{-1}	sampling rate, m^3 min^{-1}	characteristic width[a] inlet, cm	characteristic width[a] impaction surface, cm	inlet Stokes no. for 100-μm droplets	inlet Stokes no. for 100-μm droplets
passive							
Mrose (*20*)	cloth surface	ambient wind	variable		?[f]	variable	
Okita (*21*)	grid	ambient wind	variable		0.01	variable	
Lazrus et al. (*22*)	screen	ambient wind	variable		?	variable	
Sadasivan (*23*)	screen	ambient wind	variable		?	variable	
Falconer and Falconer (*24*)	grid	ambient wind	variable		0.02	variable	
active							
Houghton and Radford (*12*)	screen	600	102	30	0.01	3[c]	0.6
May (*25*)	grid	450	11	10	0.05	7[c]	1.4
May (*25*)	jet impactor	1700	0.05	0.85	0.4	?	13
Okita (*21*)	screen	94	1	7.5	?	?	0.3
Mack and Pilie (*26*)	rotating arm	1500–5000	7		0.45	?	
Katz (*7*)	jet impactor	2000	1.2	?	0.2	5[d]	?
Brewer et al. (*27*)	screen	320	1.5	5	0.02[e]	5[c]	2.0
this paper	rotating arm	3800–5600	5		0.48	20	

[a] Characteristic width of inlet: radius of circular inlet (*12*, *21*, *25b*, *27*), half-width of square inlet (*25a*). Characteristic width of impaction surfaces: radius of wires (*12*, *21*, *24*, *25a*, *27*), half-width of jet (*7*, *25b*), radius of rod (*26*, this paper). [b] Diameter of droplets collected with 50% efficiency. [c] Calculated from impaction theory for cylinders (*19*). [d] Calculated by Katz from theory and confirmed by experiment. [e] Obtained by personal communication from R. L. Brewer. [f] ? = not reported, or cannot be computed from available data.

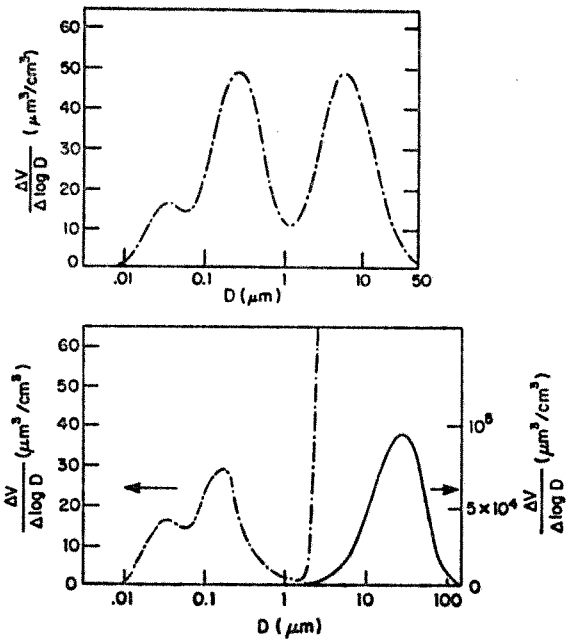

Figure 1. (Top) Typical urban aerosol size distribution profile (*1*). (Bottom) Expected shift in the size distribution profile as a result of fog formation.

diffusion. Of these, inertial separation, particularly impaction, most readily achieves sharp size cuts of a few microns and has been the method favored by past investigators. The efficiency of collection by impaction is a function of the Stokes number St (*19*):

$$\mathrm{St} = \frac{\rho_D D^2 U}{18 \mu a} \qquad (1)$$

where ρ_D is the droplet density, D is the droplet diameter, U is the velocity of approach, μ is the viscosity of air, and a is a characteristic width of the impaction surface. The size cut of a sampler is defined as the diameter D_{50} of droplets collected with 50% efficiency, and the cutoff Stokes number St_{50} is the corresponding Stokes number. Fogwater samplers used in past investigations (Table I) can be divided into two general groups: (1) passive collectors, where droplets impact on the collecting surface with the velocity of the ambient wind, and (2) active collectors, where droplets are accelerated to a certain velocity as they approach the collection surface. Passive collectors have the obvious drawback that the impaction velocity is not well-defined but instead fluctuates with the ambient wind. As a result the size cut varies with time, and the sample is not necessarily representative of the actual fogwater. Furthermore, at low wind speeds the minimum size of particles which will impact becomes large enough that the rate of sample collection becomes unacceptable, thereby precluding the use of these collectors in many locations. In active collectors, the size-dependent collection efficiency can be characterized for a given geometry of the impaction surface. However, modification of the ambient velocity of the droplets introduces two potentially important problems: perturbation of the ambient thermodynamic equilibrium and anisokinetic sampling.

Perturbation of the Ambient Thermodynamic Equilibrium. Modification of the flow field in active collectors may produce significant evaporation or condensation of the droplets as they approach the impaction surface. The total loss of water droplets has been reported past the first two stages of a cascade impactor (*25*). The extent to which droplet sizes are modified during approach can be estimated by simple mass transfer calculations, as shown in the next section. Unfortunately, no such calculations have been reported in the references of Table I.

Evaporation may also occur following collection if the droplets are not sheltered immediately from the flow of air past the impaction surface, because the air mass in a fog is thermodynamically inhomogeneous (*29*) and contains pockets of unsaturated air. Aside from evaporation, contact of the collected droplets with changing air masses may alter their compositions. It is therefore important that collected droplets be removed rapidly from the air flow. In the jet impactor designed by Katz (*7*), this is achieved with a rotating impaction surface; in the rotating arm collector, centrifugal force rapidly drives the impacted droplets into collection bottles where the air is stagnant. The screen collectors of Table I rely on gravity to draw the impacted droplets into storage bottles at the bottom of the

screen, but this is a slow process (especially in light fogs).

Anisokinetic Sampling. Recent studies of anisokinetic sampling biases (*30, 31*) have indicated that a sampler oriented into the wind can lose over 30% of particles with inlet Stokes' numbers larger than 0.5. In a crosswind, losses are considerably greater. Losses are found to be maximum for sampling velocities 2–5 times the ambient wind velocity. In addition, deposition of most particles to the walls within a few inlet diameters from the inlet has been reported for Re > 5000 (*31*).

Although moderate sampling velocities have been used in the ducted devices listed in Table I, inlet Stokes' numbers are still high in most cases. In screen and grid collectors, the moderate sampling velocities used introduce the additional problem that very thin wires are required for impaction. Because the larger droplets in the fog are then comparable in size to the radius of the impaction cylinder, interception and aerodynamic interactions between the droplets and the wires become important. The impaction characteristics are then quite different from those of the point particles considered in most theoretical treatments of impaction on cylinders. The apparent geometry of a very thin wire also changes significantly as fog droplets collect on it, introducing uncertainty in the size cut.

Proper scaling of the inlet could allow the use of high impaction velocities with little anisokinetic sampling bias. However, droplets tend to fly off collection strings at velocities higher than about 8 m s^{-1} (*12*).

The anisokineticity effect can be suppressed by eliminating the inlet and, instead, generating an apparent velocity by moving the impaction surface at high speed through the ambient air. Such devices have been used in airborne sampling of clouds (*32, 33*), where the speed of the aircraft constituted the apparent velocity. In ground-based collectors, high velocities can be generated by using a rotating system.

Design of a Rotating Arm Collector

Rotating arm collectors have been used for many years to collect biological particles on adhesive coated surfaces (*34–36*). Recently, a rotating arm virtual impactor has been developed to sample isokinetically giant atmospheric particles (*37*). In another device, the solid arms have been modified to collect fogwater by introducing a slot in the leading edges of a hollow arm (*26*). For the purpose of our field programs, we have developed an improved version of the latter collector.

Principle. The design of the rotating arm collector used in the Caltech fog sampling program is shown in Figure 2. A motor drives at high speed (1700 rpm) a type 304-L stainless steel solid rod of length $2L$ = 63 cm. Each end of the rod has a slot milled into its leading edge. Standard 30-mL VWR narrow mouth bottles are mounted at the ends of the arm to collect the water which impacts in the slots and flows outward by centrifugal force. Threaded Teflon tubes screwed onto the end of the arm and extending inside the collection bottles prevent the collected fogwater from running out after the instrument is stopped. Deflectors prevent water which impacts on the solid part of the arm from entering the slot since the collection of this water would bias the sample toward large droplet sizes. Small fins are welded to the back of the arm for extra strength. The entire arm is Teflon coated. In the absence of previous calibration data, the design was based on a cutoff Stokes number of unity. The cutoff size is weakly dependent on St_{50}; i.e., $D_{50} \propto St_{50}^{1/2}$, so even though the actual St_{50} may differ substantially from unity, the effect on D_{50} was not expected to be too large.

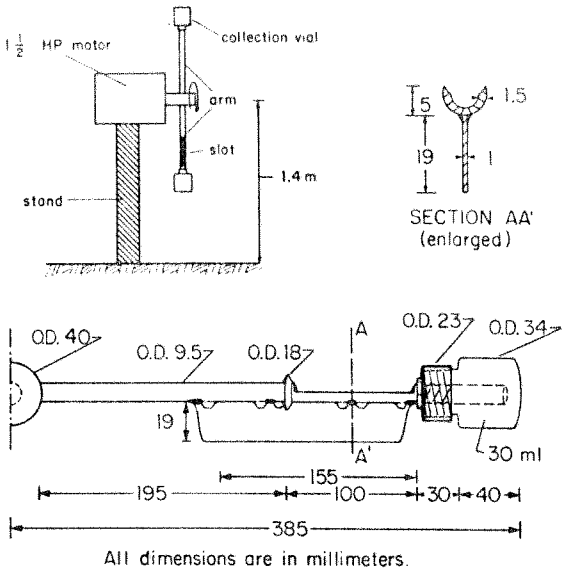

Figure 2. Caltech rotating arm collector. Full welds attaching the fin to the rod are shown in dark.

Mechanical Constraints. The size cut is determined by the choice of $(U/w)^{1/2}$, where w is the width of the slotted portion of the arm. Because reducing w leads to a proportional reduction in the sampling rate achieved with the instrument, a preferable way to obtain an acceptably low D_{50} is to operate at a high approach velocity. However, the resulting aerodynamic drag force F limits the extent to which U can be increased.

The arm consists of cylindrical sections and a half-cylinder cup. The drag coefficients C_d of these shapes at Reynolds numbers in the range 10^4–10^5 are approximately 1 and 2, respectively (*38*). The power P required to rotate the arm at a rotating speed ω (rps) is given by

$$P = 2\int_0^L \frac{dF}{dl}\, U(l)\, dl \qquad (2)$$

This may be separated into the components for the solid rod ($l < L_1$), the slot ($L_1 < l < L_2$), the bottle cap ($L_2 < l < L_3$), and the bottle ($L_3 < l < L$). Noting that the drag force is given by

$$F = C_d A \rho_a (U^2/2) \qquad (3)$$

where A is the projected area of the shape and ρ_a is the density of air, we find

$$P = 2\rho_a \omega^3 \pi^3 \sum_{i=1}^{4} C_{di} w_i (L_i^4 - L_{i-1}^4) \qquad (4)$$

where the w_i's are the widths of the corresponding portions of the arm, $L_0 = 0$, and $L_4 = L$. The power required to drive the arm is a strong function of the dimensions of the arm and the rotation frequency. To facilitate operation of the arm using readily available electrical circuits, the size and speed must be limited. Our rotating arm was designed to achieve an acceptable sampling rate and size cut, while not requiring more than a 110-V, 15-A circuit to drive the sampler. The power required when the collector is rotating at 1700 rpm is calculated from eq 4 to be 900 W. A 1.5-hp (1120-W) motor is sufficient to drive the collector, and this is still compatible with electrical circuits likely to be available in the field. The 30-mL cylindrical collection bottles are major contributors to the drag (450 W) because of their size, shape, and velocity. Collection vials are very small in the instrument described by Mack and Pilie (*26*), but the resulting samples are then too small for chemical determination, and the sampler is

inconvenient because of rapid overloading of the vials. Streamlined bottles or bottle casings could be adapted to the present design to minimize the drag while keeping the sample volume large enough to make the instrument practical.

Specifications. The slot velocities range from 38 to 56 m s^{-1}, and the Reynolds numbers at the slots range from 24 000 to 35 000. Laboratory tests under zero wind conditions indicate that air is drawn through both faces of the collector at a velocity of 1.5 m s^{-1} roughly uniform across the plane of collection (measured 25 cm away from the plane of collection). The sampled air is expelled radially (velocity of 4 m s^{-1} measured 25 cm away from the tip). This induced flow ensures that the sampled air is entirely renewed at every half-rotation of the arm, so that the sampling rate is 5 m^3 of air/min. Assuming 100% efficiency, a collection rate of 0.5 mL min^{-1} would be achieved in a fog of 0.1 g m^{-3} liquid water content. Collection rates of up to 2 mL min^{-1} have been obtained in the field.

Droplet Evaporation. Droplet evaporation may occur at the three stages of collection: (1) as the droplet approaches the impaction surface, (2) in the collection slots, and (3) in the collection bottles.

Evaporation during approach is most likely to occur as the droplet approaches the slot at high apparent velocity. Let us consider, as a worst case, the stagnation streamline; as air approaches the slot its velocity decreases from U_∞ in the free stream to 0 at the stagnation point. This deceleration leads to aerodynamic heating. We write the appropriate equations for mass transfer (*16*) and droplet trajectory: because we are concerned only with activated supermicron droplets, we neglect the effect of solutes on the physical properties of the droplets.

$$r\frac{dr}{dt} = \frac{s - y(T)}{\dfrac{\rho_W RT}{e_{sat}(T)DM_r} + \dfrac{\Delta H \rho_W}{kT}\left(\dfrac{\Delta H M_r}{RT} - 1\right)} \tag{5}$$

$$y(T) = \frac{2\sigma M_r}{RT\rho_W r}$$

$$\frac{dz}{dt} = -U_D \tag{6}$$

$$\frac{dU_D}{dt} = -\frac{3}{8}\left(\frac{\rho_a}{\rho_W}\right)C_d\frac{(U_D - U)^2}{r} \tag{7}$$

r is the droplet radius; $s = (e/e_{sat}(T)) - 1$ is the ambient supersaturation, where e is the water vapor pressure over the droplet and $e_{sat}(T)$ is the saturation water vapor pressure over a plane water surface at temperature T; σ is the surface tension of water against air; R is the universal gas constant; ρ_W and ρ_a are the densities of water and air, respectively; D is the diffusivity of water vapor in air; ΔH is the latent heat of vaporization of water; k is thermal heat conductivity of air; M_r is the molecular weight of water; z is the distance of the droplet to the collector; U is the velocity of the air flow; U_D is the velocity of the approaching droplet. The local Reynolds number Re_1 of the droplet is

$$Re_1 = \frac{2|U_D - U|r}{\nu} \tag{8}$$

where ν is the kinematic viscosity of air. The drag coefficient C_d can be approximated for $Re_1 < 10^3$ by (*39*)

$$C_d = \frac{24}{Re_1}(1 + 0.158Re_1^{2/3}) \tag{9}$$

Under the assumption that the compression proceeds isentropically, the temperature and pressure fields for the approaching droplet are given by

$$T = T_\infty + \frac{U_\infty^2 - U^2}{2c_p} \tag{10}$$

$$P = P_\infty\left(\frac{T}{T_\infty}\right)^{\gamma/(\gamma-1)} \tag{11}$$

where c_p is the specific heat of air at constant pressure and γ is the ratio of specific heats. The water vapor pressure is calculated by assuming that the mixing ratio of water vapor remains constant as the air approaches the collector and that droplets in the free stream are at equilibrium with water vapor:

$$e(T) = \frac{P}{P_\infty}e_{sat}(T_\infty)[1 + y(T_\infty)] \tag{12}$$

For a given $U(z)$ along the stagnation streamline, the coupled eq 5–7 can readily be solved numerically. Unfortunately, the complicated potential flow around a cup has not yet been characterized to the authors' knowledge. It is assumed here that the flow (at least to within some distance of the impaction surface) should be comparable to that around a cylinder of diameter w, for which the potential flow solution along the stagnation streamline yields

$$U = U_\infty\left[1 - \left(\frac{w}{2z}\right)^2\right] \tag{13}$$

The system of eq 5–7 is then integrated with a fourth-order Runge–Kutta routine. Under the conditions U_∞ = 56 m s^{-1}, T_∞ = 283 K, and P_∞ = 1 atm, the percentage of loss in droplet mass by the time the droplet reaches the stagnation point (actually the time at which $(2z - w)/w < 0.001$) is less than 0.1% for activated supermicron droplets. Increasing U_∞ to 100 m s^{-1} does not significantly increase this loss; therefore, evaporation during approach to the slots is not a constraint in choosing higher approach velocities.

A similar mass transfer calculation was conducted to evaluate the effect of thermodynamic modifications as air is drawn through the sampler with a velocity U = 1.5 m s^{-1}. It was found that no significant change in droplet size occurs for supermicron droplets during that stage of approach.

Evaporation in the slot could also occur after impaction from the thin film of water in the slot to the unsaturated air above. Because the flow patterns in the slot originate mostly from turbulent eddies, an accurate description of the transfer phenomena would be very complicated. By using an oversimplified model of tangential flow of unsaturated air over a flat plate, we estimated that under the worst conditions the evaporation rate could be no more than 0.01 g min^{-1}. Even in this case, evaporation is still very small at typical collection rates (0.1–1 g min^{-1}).

Finally, evaporation in the collection bottles must be considered. As a test, the bottles were filled halfway with water (15 mL in each), mounted on the collector, and spun for 30 min in a dry atmosphere. This did not affect the volume of water in the bottles, which shows that evaporation in the bottles is negligible.

Safety. Safety is a primordial concern for a large diameter device rotating in the open. The collector must be carefully balanced to prevent vibrations and securely mounted to a rigid stand. The mechanisms for mounting the bottles must be able to withstand the loads due to high acceleration (1200g). Stainless steel caps with close tol-

erance threads were found to be satisfactory in laboratory tests. The operating site must be carefully selected and supervised to minimize the hazard.

The arm must be inspected to detect any mechanical flaws or stress concentration points which could lead to failure by fatigue. In the original design of the collector (*8*), the back fin was attached to a 304 steel rod with tack welds. This method of attachment produced a sharp angle with the rod, which served as an incipient crack. Stress concentration at that point led to one occasion of failure by fatigue. To prevent this from reoccurring we have modified the design of the fins; the points of contact with the rod are now smooth and fully welded. We have switched to 304-L steel, which is less prone to weakening at the weld points. Also, the instrument is now stress-relieved after welding to further reduce the risk of failure.

Calibration

Mack and Pilie (*26*) used theoretical results for impaction on cylinders to predict the collection efficiency of their rotating arm collector. However, they presented no justification for doing so. Because of the complicated flow inside the cavity, impaction in the slot may differ from impaction on a cylinder. Experimental calibration is necessary.

Scaling Considerations. At high flow Reynolds numbers and low interception numbers, the collection efficiency, η, of an impaction surface can be satisfactorily reduced to a function of the three dimensionless groups St, Re_D, and Mach number (*19*). Re_D is the droplet Reynolds number based on the droplet diameter and the free-stream velocity. When the Mach number based on the local sonic speed is smaller than 0.4, it has a negligible effect on the collection efficiency (*40*). As a good approximation

$$\eta = f(\mathrm{St}, \mathrm{Re_D}) \tag{14}$$

In the range $10^0 < Re_D < 10^3$, which is the range at which the droplets are collected in the slots, η is a strong function of both St and Re_D (*19*). To reduce the dependence of η to one dimensionless group, Israel and Rosner (*28*) have proposed a generalized Stokes number which accounts for the variation in the droplet drag coefficient at higher particle Reynolds numbers:

$$\mathrm{St}' = \frac{4}{3}\left(\frac{\rho_D}{\rho_a}\right)\left(\frac{D}{a}\right)\int_0^{\mathrm{Re_D}} \frac{d\mathrm{Re}'}{C_d(\mathrm{Re}')\mathrm{Re}'} \tag{15}$$

The generalized Stokes number reduces to the Stokes number for $Re_D \ll 1$. For higher particle Reynolds numbers St′ is related to St by

$$\mathrm{St}' = \mathrm{St}\psi(\mathrm{Re_D}) \tag{16}$$

where

$$\psi(\mathrm{Re_D}) = \frac{24}{\mathrm{Re_D}}\int_0^{\mathrm{Re_D}} \frac{d\mathrm{Re}'}{C_d(\mathrm{Re}')\mathrm{Re}'} \tag{17}$$

By substitution of St′ for St, the dependence of η on Re_D is reduced (*28*), so that the collection efficiency is a function of St′ alone, i.e.

$$\eta \simeq f(\mathrm{St}') \tag{18}$$

Calibration Method. Calibration of an aerosol sampling device involves dispersal of a calibration aerosol in a large volume of air under well-controlled conditions and would generally be conducted in a wind tunnel. Since a wind tunnel suitable for the rotating arm collector, or even a scaled-down version of the instrument, was not available, an alternate approach was taken. This method, which has recently been used to test sampler inlets (*41*), allows evaluation of the performance of the instrument under ambient conditions.

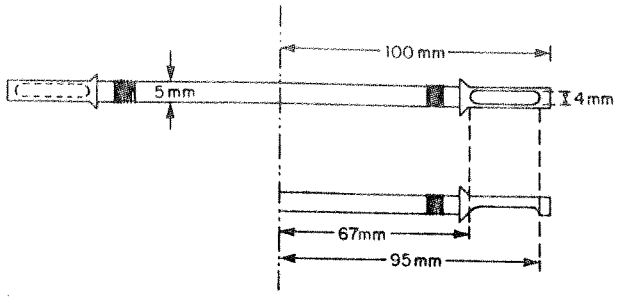

Figure 3. Model rotating arm collector used in calibration experiment.

A tracer gas is used to follow an aerosol plume as it is advected in the atmosphere from an aerosol generator to the collector to be tested. A chemically tagged monodisperse aerosol is released at a constant rate together with a tracer gas. The collection device is set one meter downwind of the point of release and samples the diluted aerosol plume. Prior to testing, the concentration of aerosol at the release point is measured. During testing, tracer gas samples are taken at the release point and next to the impaction surface of the sampler. Automatic continuous gas samplers give integrated measurements of tracer gas concentrations at both locations throughout the testing interval. If sedimentation of the particles is insignificant over the distance from the release point to the sampler, the trajectories of the particles and the gas are nearly identical over that distance. The average concentration C of aerosol crossing the collector path is then given by

$$C = C_0\left(\frac{C^*}{C^*_0}\right) \tag{19}$$

where the subscript 0 refers to the release point and the asterisk refers to the tracer gas. If a mass m of aerosol is collected by the sampler over a time interval Δt with a sampling rate Q, the collection efficiency is

$$\eta = \frac{m}{CQ\Delta t} \tag{20}$$

By running several tests over a range of St′ values, one obtains the dependency of η on St′.

In our tests a monodisperse sodium fluorescein solid aerosol was generated with a Berglund–Liu Model 3050 vibrating orifice generator. Sulfur hexafluoride (SF_6) was used as a tracer gas and connected to the upstream of the dilution air system of the aerosol generator (for which the flow rate was about 40 L min^{-1}) to ensure complete mixing. The aerosol production rate ranged from 10^{-9} to 10^{-7} g min^{-1}, and the flow rate of SF_6 ranged from 0.43 to 0.68 cm^3 min^{-1}. Due to the slow rate of aerosol release, the prototype collector had to be scaled down so that sufficient amounts of aerosol could be conveniently collected for analysis. The model collector (Figure 3) consists of two slotted ends screwed onto a solid rod. It was spun with a variable speed 0.5-hp 10000 rpm motor. Similarity of the Reynolds numbers was maintained, and the aspect ratio was kept as close as possible to that of the prototype. For structural reasons the width/length ratio for the slots is 0.15 in the model, whereas it is 0.095 in the prototype.

The experimental setup is shown in Figure 4. A fan generating a wind speed of about 5 m s^{-1} was used to advect the aerosol toward the collector. The experiments were conducted under conditions of low ambient winds. Dilution of the plume from the point of release to the

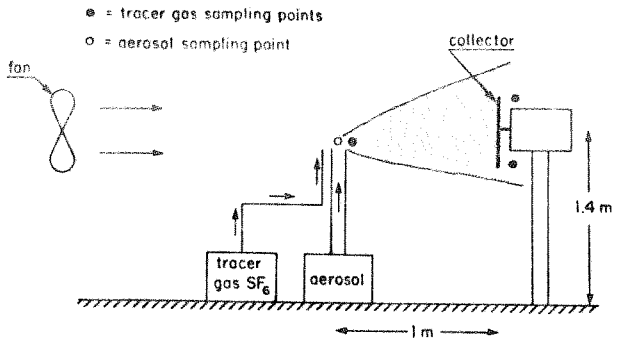

Figure 4. Calibration experiment setup.

sampling point, as measured by C^*/C^*_0, ranged from a factor of 30 to 1000 depending on the meteorological conditions. Particles ranging in diameter from 3 to 20 μm were generated to cover a wide range of Stokes numbers. The settling velocity of 20 μm particles is less than 1 cm s^{-1}, so that sedimentation is negligible over the distances of concern. Tests were run over 30-min intervals, which allowed collection of a sufficient amount of aerosol for accurate determination of the collected mass.

Two automatic continuous gas samplers, sampling over 5-min intervals, and one syringe pump, sampling over 30-min intervals, were used to obtain SF_6 samples. Comparison of the 5- and 30-min integrated measurements provided a check on the SF_6 levels and raised attention to any major changes in the ambient wind speed or turbulence over the course of testing. Analysis was done by gas chromatography using an electron capture detector (*42*). Samples were diluted to reach the optimal SF_6 detection range (100–300 ppt (parts per trillion)). The aerosol concentration at the release point was measured prior to testing by running a known volume of air through a glass-fiber filter. To restrict the aerosol loading on the model arm to the collecting slots, all other parts of the collector were covered with tape, which was removed prior to analysis. A coat of Vaseline grease was applied on one of the two slots to test against possible particle bounce-off. After testing, the sodium fluorescein was extracted in an ultrasonic bath for 30 min with a 0.1 N NH_4OH solution. For the greased slots extraction was first carried out with toluene for 30 min and then with the 0.1 N NH_4OH solution for another 30 min. The aqueous phase was then separated by centrifugation. The sodium fluorescein was analyzed by spectrofluorometry.

Results and Discussion. Figure 5 shows the observed dependence of the collection efficiency on St′ for the scaled-down model. The scale below the abscissa gives the droplet diameter as a function of St′ for a droplet impacting at the middle of the slot in the full-scale arm. Although there is some scatter in the data around $\eta = 50\%$, St'_{50} (based on the data from the greased slots) is about 5, which corresponds to $D_{50} = 20$ μm. Ungreased surfaces collect particles with lower efficiency, which indicates that some particle bounce-off occurs.

Each collection efficiency measurement corresponds to a range of Stokes numbers because velocities of approach vary from one end of the slot to the other. The spread in the Stokes numbers in the scaled-down model is 17% in each direction off the middle of the slot. In the prototype this spread is 19%, which leads to a 10% uncertainty on the size cut of the instrument. A way to eliminate this uncertainty would be to use a tapered slot, i.e., narrow close to the shaft and widening toward the tip, to maintain St′ constant over the whole length of the slot.

In ref 28, it is claimed that the use of St′ in interpreting inertial impaction on a surface greatly reduces the dependence of η on the geometry of that surface. Comparison of our calibration data to the curve obtained in ref 28 from previous calculations for cylinders and spheres shows similarity in shape, but our results are shifted toward the higher Stokes numbers (Figure 5). Because the largest discrepancies occur at low St′ values, this is not likely due to particle bounce. Recent studies of virtual impactors (*43*) have suggested an explanation for the larger St'_{50} in the rotating arm collector. In order to be collected, the particles must not only pass the virtual surface through which there is no mean air flow but also penetrate through the air in the cavity to reach the wall of the collector. Those particles which do not impact on the walls have a significant probability of being reentrained, particularly in the rotating arm collector where there is an induced flow along the length of the collector slot. This may explain the large Stokes numbers required for efficient collection.

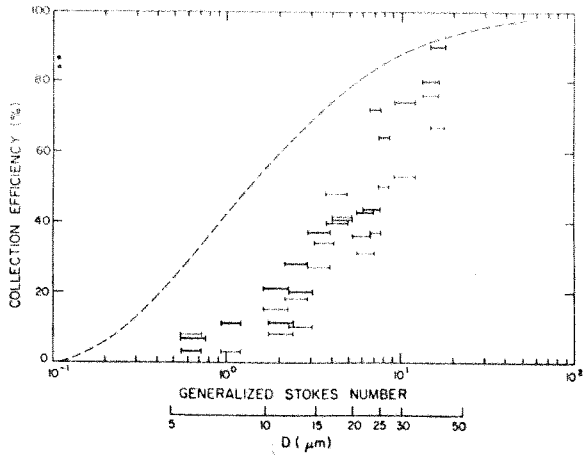

Figure 5. Collection efficiency of model collector vs. the generalized Stokes number, for greased (in bold) and ungreased impaction surfaces. The scale below the abscissa converts the generalized Stokes number to the diameter of droplets impacting in the middle of the slots of the prototype collector. The dashed curve represents theoretical collection efficiencies for cylinders and spheres (*28*).

Comparison with Field Results. Some liquid water content data were obtained at Bakersfield, CA, in Jan 1983 by drawing air with an open-faced Hi-Vol sampler through a paper filter. By measuring the difference in weight of the filters after a certain volume of air has been drawn through the Hi-Vol, one obtains an estimate of the liquid water content. At another location (Albany, NY, Oct 1982) the liquid water content was determined by infrared scattering using a laser transmissometer (*44*). It must be noted that uncertainties as large as 50% are commonly associated with these two liquid water content measurement methods. Figure 6 compares the amount of water collected per cubic meter of air sampled (assuming a sampling rate of 5 m^3 min^{-1}) to the actual liquid water content measured independently. A best fit to the data indicates an overall collection efficiency of 60%. The apparent decrease in collection efficiency when the liquid water content is high may be due to overloading of the bottles before the collector was stopped. To prevent premature overloading due to air lock in the bottles, we have since then added a small hole (0.36-mm diameter) on the upper part of the Teflon tube extending inside the bottle. This allows exchange of air in and out of the bottle during sampling and has been found to improve the collection characteristics in dense fog.

Conclusion

The performance of instruments to collect fogwater for chemical analysis can be assessed in the light of the fol-

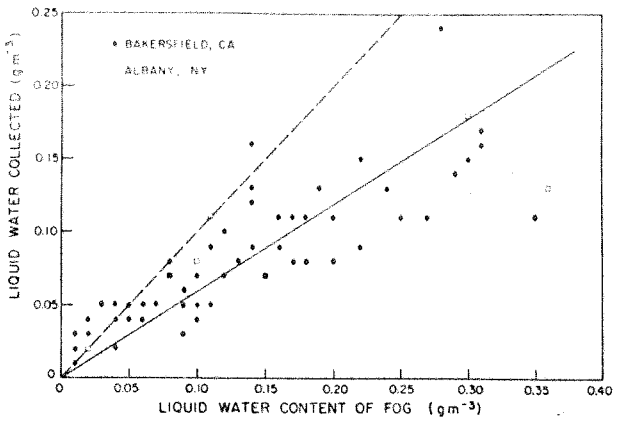

Figure 6. Collected water per cubic meter of air sampled vs. liquid water content. Liquid water content was measured with an open-faced Hi-Vol sampler (Bakersfield, CA) or with an infrared laser transmissometer (Albany, NY). (—) Linear best fit to the data. (---) 100% collection efficiency line.

lowing design criteria: (a) high collection efficiency for droplets in the size window 1–100 μm, (b) collection rate high enough to supply the sample volume required for chemical analysis, (c) conservation of droplet size during approach to the collection surface, and (d) rapid removal of the collected droplets away from the air flow into a quiescent environment.

We discussed in depth the design and characteristics of the rotating arm collector used in our ongoing fogwater chemistry field program and concluded that it performs well in preserving the chemical integrity of the collected droplets while providing large sample volumes. These results have been confirmed in the field (*6*). An in situ calibration indicated a size cut of 20 μm diameter, which is significantly higher than that desired. Because our sampler and the jet impactor designed by Katz (*7*) give consistent determinations of ionic concentrations in fogwater, there appears to be no obvious dependence of the chemical composition on the size of droplets collected. The rotating arm seems to collect samples representative of the fogwater chemistry in spite of its high lower size cut.

Our laboratory is currently investigating several promising designs of fogwater samplers that will collect efficiently droplets in the 1–10-μm size range while minimizing potential sample contamination. The objective is to build a reliable, fully automated instrument suitable for routine monitoring under a wide variety of field conditions. Results will be presented in a future report.

Acknowledgments

E. F. Daly and J. J. Fontana constructed the collectors and provided many valuable practical suggestions. Comments from D. S. Wood, J. M. Waldman, J. W. Munger, and M. R. Hoffmann are gratefully acknowledged.

Literature Cited

(1) Whitby, K. T. *Atmos. Environ.* **1978**, *12*, 135–159.
(2) Waldman, J. M.; Munger, J. W.; Jacob, D. J.; Flagan, R. C.; Morgan, J. J.; Hoffmann, M. R. *Science (Washington, D.C.)* **1982**, *218*, 677–680.
(3) Munger, J. W.; Jacob, D. J.; Waldman, J. M.; Hoffmann, M. R. *J. Geophys. Res.* **1983**, *88*, 5109–5123.
(4) Watson, H. H. *Am. Ind. Hyg. Assoc., Q.* **1954**, *15*, 21–25.
(5) Jacob, D. J.; Waldman, J. M.; Munger, J. W.; Hoffmann, M. R. *Tellus*, in press.
(6) Hering, S. V.; Blumenthal, D. L. "Fog Sampler Intercomparison Study: Final Report". Prepared for Coordinating Research Council, Atlanta, GA, 1984, Project STI 11 90063.
(7) Katz, U. "Communications de la 8eme Conference sur la Physique des Nuages". Clermont-Ferrand, France, July 15–19, 1980.
(8) Jacob, D. J.; Flagan, R. C.; Waldman, J. M.; Hoffmann, M. R. *Proc. Int. Conf. Precipitation Scavenging, Dry Deposition, Resuspension, 4th* **1983**, 125–136.
(9) Junge, C.; McLaren, E. *J. Atmos. Sci.* **1971**, *28*, 382–390.
(10) Jacob, D. J.; Hoffmann, M. R. *J. Geophys. Res.* **1983**, *88*, 6611–6621.
(11) Bassett, M.; Seinfeld, J. H. *Atmos. Environ.* **1983**, *17*, 2237–2253.
(12) Houghton, J. G.; Radford, W. H. *Pap. Phys. Ocean. Met. Mass. Inst. Technol. Woods Hole Ocean. Inst.* **1938**, *6* (4).
(13) Garland, J. A. *Q. J. R. Meteorol. Soc.* **1971**, *97*, 483–494.
(14) Mallow, J. V. *J. Atmos. Sci.* **1975**, *32*, 440–443.
(15) Goodman, J. *J. Appl. Meteorol.* **1977**, *16*, 1056–1067.
(16) Pruppacher, H. R.; Klett, J. D. "Microphysics of Clouds and Precipitation"; Reidel: Dordrecht, Netherlands, 1978; pp 141–142, 418–421.
(17) Roach, W. T. *Q. J. R. Meteorol. Soc.* **1976**, *102*, 355–359.
(18) Gerber, H. E. *J. Atmos. Sci.* **1981**, *38*, 454–458.
(19) Friedlander, S. K. "Smoke, Dust and Haze"; Wiley: New York, 1977; pp 95–109.
(20) Mrose, H. *Tellus* **1966**, *18*, 266–270.
(21) Okita, T. *J. Meteorol. Soc. Jpn.* **1968**, *46*, 120–126.
(22) Lazrus, A. L.; Baynton, H. W.; Lodge, J. P. *Tellus* **1970**, *22*, 106–114.
(23) Sadasivan, S. *Atmos. Environ.* **1980**, *14*, 33–38.
(24) Falconer, R. E.; Falconer, P. D. *J. Geophys. Res.* **1980**, *85*, 7465–7470.
(25) May, K. R. *Q. J. R. Meteorol. Soc.* **1961**, *87*, 535–548.
(26) Mack, E.; Pilie, R. U.S. Patent 3 889 532, 1975.
(27) Brewer, R. L.; Ellis, E. C.; Gordon, R. J.; Shephard, L. S. *Atmos. Environ.* **1983**, *17*, 2267–2271.
(28) Israel, R.; Rosner, D. E. *Aerosol Sci. Technol.* **1983**, *2*, 45–51.
(29) Roach, W. T.; Brown, R.; Caughey, S. J.; Garland, J. A.; Readings, C. J. *Q. J. R. Meteorol. Soc.* **1976**, *102*, 313–333.
(30) Durham, M. D.; Lundgren, D. A. *J. Aerosol Sci.* **1980**, *11*, 179–188.
(31) Davies, C. N.; Subari, M. *J. Aerosol Sci.* **1982**, *13*, 59–71.
(32) Petrenchuk, O. P.; Aleksandrov, N. N. *Glavnoi Geofiz. Obs., Leningr. Tr.* **1966**, *185*, 126–132.
(33) Mohnen, V. A. *Atmos. Technol.* **1980**, *12*, 20–25.
(34) Durham, O. C. *J. Allergy* **1947**, *18*, 231–238.
(35) Perkins, W. A. Stanford University, Palo Alto, CA, 1957, second semiannual report.
(36) Asai, G. N. *Phytopathology* **1960**, *50*, 535–541.
(37) Hameed, R.; McMurry, P. H.; Whitby, K. T. *Aerosol Sci. Technol.* **1983**, *2*, 69–78.
(38) Hoerner, S. "Fluid-Dynamic Drag"; Hoerner Fluid Dynamics: Brick Town, NJ, 1965; pp 3/9, 3/17.
(39) Serafini, J. S. 1954, NACA Report 1159.
(40) Biswas, P.; Flagan, R. C. *Environ. Sci. Technol.* **1984**, *18*, 611–616.
(41) Hofschreuder, P.; Vrins, E.; van Boxel, J. *J. Aerosol Sci.* **1983**, *14*, 65–68.
(42) Drivas, P. J.; Shair, F. H. *Atmos. Environ.* **1974**, *8*, 1155–1163.
(43) Biswas, P., California Institute of Technology, Pasadena, CA, personal communication, 1983.
(44) Jiusto, J. E.; Lala, G. G. State University of New York at Albany, Albany, NY, 1983, ASRC-SUNY Publication 869.

Received for review August 8, 1983. Accepted May 15, 1984. This research was funded by the California Air Resources Board (A2-048-32) and the President's Fund of the California Institute of Technology.